Modelling of Casting, Welding, and Advanced Solidification Processing XI

NON-MONOTONE TEMPERATURE BOUNDARY CONDITIONS IN DENDRITIC GROWTH

Martin E. Glicksman[1], John S. Lowengrub[2], Shuwang Li[2]

[1]Rensselaer Polytechnic Institute, Materials Science & Engineering Department; Troy, NY 12180-3590, USA
[2]University of California at Irvine, Department of Mathematics; Irvine, CA, 92697-3875, USA

Keywords: dendrites, side branching, solidification, fundamentals

Abstract

When the Gibbs-Thomson-Herring anisotropic capillary boundary condition is applied at the solid-liquid interface of a crystallite with shape anisotropy, such as a needle crystal or dendrite, the interface can develop periodic non-monotone temperature distributions. This surprising result was discovered recently for the case of a slender ellipsoidal crystallite with its solid-melt interfacial energy parameters chosen equivalent to those for pivalic acid—a crystal exhibiting 4-fold anisotropy of its interfacial energy. An unexpected deep minimum develops in the equilibrium temperature close to the highly curved tip. This minimum results in the tip temperature itself becoming warmer than the adjacent interface, thereby further steepening the local temperature gradient at the tip relative to nearby gradients. Numerical simulations of the solidification dynamics, using a spectrally accurate, two-dimensional boundary integral method, show that a non-monotonic temperature distribution anywhere along the crystal-melt interface leads to localized negative curvatures and, eventually, to periodic oscillations in the temperature and tip shape. Periodic changes in the tip shape and temperature distribution lead to growing protuberances that form side branches. The dynamical process acts as a "limit cycle", stimulating a chain of wave-like disturbances behind the tip that grow sequentially and form the periodic side-branches of a dendrite. What is especially significant about these observations is that perturbations are not needed to "destabilize" the solid-melt interface, and the dendritic pattern evolves in a deterministic manner. Selective amplification of interfacial noise—the conventional explanation of dendrites—does not play an important rôle in this process, so long as sufficient shape and interfacial energy anisotropy occur together.

Background

Dendritic transport length scales were established almost 60 years ago in a classical analysis by G.P. Ivantsov [1]. Ivantsov showed in the case of a pure melt that the product of the dendritic tip speed, V, with the tip radius of curvature, R, could be related to the supercooling, $T_m - T_\infty$, where T_m is the bulk melting point, and T_∞ is the temperature of the melt far away from the interface. Specifically, Ivantsov showed that for the case of a branchless needle-dendrite, which he modeled as a paraboloid of revolution,

$$(T_m - T_\infty) = \frac{\Delta H_f}{C_p} P e^P \mathrm{Ei}(P), \tag{1}$$

where C_p and ΔH_f are the molar specific heat of the melt, and the molar latent heat of fusion, respectively, and $P \equiv VR/2\alpha$ is the thermal Péclet number for a pure substance, or the solutal Péclet number for an alloy. The term $\mathrm{Ei}(P)$ is the first exponential integral, a tabulated function. The parameter α appearing in Eq. (1) denotes either the thermal or solutal diffusivity. Note that the only length scale within Eq. (1) is dendritic the tip radius, R, parameterized through the Péclet number. Of course, Eq. (1) provides only a relationship between the product $R \times V$, and the melt supercooling, so a second independent equation relating either V or R to the supercooling is required if one is to obtain an unique mathematical solution to the dendritic growth problem. Assessing this issue has taken many years [2]-[6], and the interested reader can consult reviews written on the subject of dendritic growth kinetics [7, 8]. The prevailing view today is that capillarity phenomena at the crystal-melt interface provide the second independent relationship in addition to Ivantsov's transport solution [9]. Although several models of dendritic growth kinetics exist today, [10]-[14], essentially all of them choose as the independent "second relationship" the dependence of the "marginal" wavenumber, $k^\star$, or critical perturbation wavelength, $\lambda^\star$, on tip speed, which dependences are found from linear stability theory [15] as

$$k^\star = \frac{2\pi}{\lambda^\star} = \sqrt{\frac{V}{2\alpha d_0}}. \tag{2}$$

Here interfacial capillarity is introduced through a microscopic length scale called the "capillary length", d_0, usually defined as

$$d_0 \equiv \frac{C_p T_m \gamma_{s\ell} \Omega}{\Delta H_f} \approx 10^{-7}\mathrm{cm}. \tag{3}$$

In Eq. (3), $\gamma_{s\ell}$ is the interfacial free energy per unit area, and Ω is the molar volume of the crystal. The scaling law that arises from such a "stability analysis" is extracted by squaring both sides of Eq. (2) and solving for the "scaling constant", $\sigma^\star \equiv \frac{1}{4\pi^2}$, which yields the prediction that

$$\sigma^\star = \frac{2\alpha d_0}{V\lambda^{\star 2}}. \tag{4}$$

Now, if one assumes (as only a rough approximation) that the critical interfacial perturbation wavelength $\lambda^\star \approx R$, and then substitutes this weak equality back into Eq. (**??**), one obtains a key dendritic scaling law, namely,

$$\sigma^\star = \frac{2\alpha d_0}{VR^2} \approx 0.025. \tag{5}$$

The validity of Eqs. (4) and (5), that $VR^2 = \text{const.}$, was checked experimentally by Glicksman et al. [16], and by Lacombe et al. [17]. These investigators analyzed dendritic growth observed under microgravity conditions, where melt convection is negligible. The verification of the dendritic scaling law that $VR^2 = \text{const.}$ is often accepted as "proof" of the combined elements contributing to dendritic growth theory: 1) Ivantsov's transport solution, Eq. (1); and 2) capillarity effects occurring at the crystal-melt interface, as expressed through either interfacial stability or solvability theories.

We now show that a completely different theoretical approach than those mentioned in (2) above might explain the action of interfacial capillarity in dendritic pattern formation.

Gibbs-Thomson-Herring Boundary Condition

GTH in Two Spatial Dimensions, $\mathbb{R}^2$

The anisotropic version of the well-known Gibbs-Thomson relationship, which connects the chemical potential with the curvature of an interface, κ, is the Gibbs-Thomson-Herring equation (GTH). The equilibrium temperature at a point on a crystal-melt interface separating pure phases in $\mathbb{R}^2$ is

$$T_e(\kappa) = T_m \left(1 - \frac{\Omega}{\Delta H_f} \left(\gamma_{s\ell} + \gamma_{\theta\theta}\right) \kappa(\theta)\right), \tag{6}$$

where the term $\gamma_{\theta\theta} \equiv \frac{\partial^2 \gamma_{sl}}{\partial \theta^2}$ is the torque, or interfacial "stiffness," and θ is the azimuthal angle, positioning the interface normal at that point. The crystal-melt interfacial energy densities of cubic crystals, $\gamma_{s\ell}$, exhibit four-fold rotational symmetry about each of the six equivalent [100] zone axes, along which cubic dendrites grow. In $\mathbb{R}^2$, if a "cubic"—i.e., a 4–fold symmetric— dendrite grows in a $\langle 100 \rangle$-type direction, for which $\theta = 0, \pm\pi/2$, and π, the anisotropic free energy per unit length along the interface may be written as

$$\gamma_{s\ell} = \gamma_0 \left(1 + \eta \cos 4\theta\right), \tag{7}$$

where γ_0 is the modulus of the interfacial free energy, and η is the amplitude of the 4-fold anisotropy. Substituting Eq. (7) into Eq. (6) and evaluating the "stiffness" term yields an expression for the dimensionless temperature shift caused by interfacial curvature in two dimensions,

$$\frac{T_m - T_e(\kappa)}{T_m} = \frac{\gamma_0 \Omega}{\Delta H_f} \left(1 - 15\eta \cos 4\theta\right) \kappa(\theta). \tag{8}$$

Equilibrium

Implementation of the GTH boundary condition for total thermodynamic equilibrium in $\mathbb{R}^2$ requires specification of Eq. (8) on the solid-melt interface of a crystallite of fixed area. The resultant constrained equilibrium shape—called the Wulff shape—mimics the polar plot of $\gamma_{s\ell}$. This closed shape provides a uniform equilibrium temperature and chemical potential at all points along the crystal-melt boundary.

Shape Anisotropy

When the GTH boundary condition is applied to a crystallite with "shape anisotropy", that is, to a slender, needle-like form, the equilibrium temperature distribution cannot remain isothermal, but, curiously, can even become non-monotonic! For specificity, we choose a parabolic interface on which to apply the GTH boundary condition. This parabola may be expressed in a standard quadratic form,

$$\frac{y}{a} = \frac{1}{2} - \frac{x^2}{a^2}. \tag{9}$$

Here the size scale of the parabolic needle is set by its tip radius, $a/2$. The curvature, κ, at any point along the parabolic interface is easily shown to be

$$\kappa = \frac{2}{a} \left(1 + \frac{4x^2}{a^2}\right)^{-\frac{3}{2}} = \frac{2}{a} \cos^3 \theta. \tag{10}$$

Substituting the parabola's curvature, Eq. (10), into the GTH boundary condition, Eq. (8), yields the expected interfacial equilibrium temperature distribution,

$$T_e(\theta) = T_m - \frac{2T_m\Omega\gamma_0}{a\Delta H_f}(1 - 15\eta\cos 4\theta)\cos^3\theta, \tag{11}$$

or, equivalently, the dimensionless temperature shift

$$\frac{T_e(\theta) - T_m}{T_m} = -\frac{2\gamma_0\Omega}{a\Delta H_f}(1 - 15\eta\cos 4\theta)\cos^3\theta. \tag{12}$$

Equation (12) shows that the temperature distribution along the crystal-melt interface depends on the anisotropy coefficient, η, as well as on the crystallite's shape and tip radius. Normalized interfacial temperature distributions corresponding to several values of η are displayed in Fig. 1. Surprisingly, the temperature distribution shown in Fig. 1, as the parabolic tip is approached ($\theta \to 0$), is non-monotonic, provided that $\eta \geq 1/95$. Moreover, as the anisotropy increases, and $\eta \to 0.066$, the tip becomes increasingly warmer than the surrounding region of the crystal-melt interface, with the tip temperature rising towards the melting temperature of a *flat* interface, T_m. The remarkable implications for this non-monotonicity will be discussed in the next section.

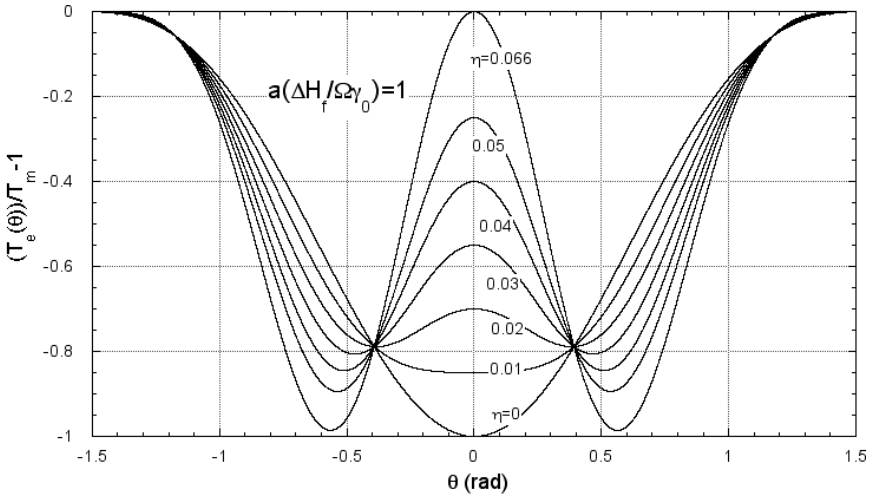

Figure 1: Relative temperature shift along the parabolic interface parameterized by the azimuthal or normal angle, θ. The actual boundary temperature shift induced by capillarity is proportional to the melting temperature, T_m, and inversely proportional to the parabola's length scale, a. These curves are plotted for $\frac{2\gamma_0\Omega}{a\Delta H_f} = 1$. When the anisotropy parameter is small ($\eta < 1/95$) the interface temperature remains monotone down as the tip is approached. For larger anisotropy coefficients the temperature becomes non-monotonic, with a distinct maximum developing at the tip, and symmetrical minima positioned a short distance away from the parabolic tip. The maximum tip temperature increases as $\eta \to 1/15 \approx 0.066$, which is the largest value permissible for a 4-fold anisotropy coefficient, η, if all interfacial orientations in the range $-\pi/2 \leq \theta \leq \pi/2$ are present. Any higher anisotropy would induce some equilibrium faceting, implying a range of "missing" orientations along the interface. Minimum tip temperature occurs at the tip, $\theta = 0$, for isotropic surface energy, $\eta = 0$.

Dynamic Phenomena

The influence of the anisotropic GTH boundary condition on dendrite dynamics can be studied using both sharp interface and phase-field techniques. We have studied dendritic quasi-steady growth dynamics using a spectrally accurate boundary integral scheme [18, 19, 20]. An important new feature of this scheme is that dynamical rescaling is used in both space and time, $\bar{\mathbf{x}} = \bar{R}(\bar{t})\mathbf{x}$, $\bar{t} = \int_0^t \frac{dt'}{R^2(t')}$, respectively, where $\bar{R}(\bar{t}) = R(t(\bar{t}))$, and $\bar{\mathbf{x}}(\bar{t})$ is the position vector of the scaled interface, and $\bar{t}$ is the re-scaled time variable. The particular scaling, $\bar{R}$, was chosen such that the total area enclosed by the scaled crystal-melt interface remains constant in time. In the time scale, $\bar{t}$, the crystal size grows exponentially.

The initial crystal shape selected was an ellipse with a major axis, C, to minor axis, A, ratio of $C/A = 2$, with a small anisotropy coefficient of $\eta = 0.005$. Growth is simulated under the influence of a constant far-field heat flux. Since the starting crystal "seed" is itself two-fold symmetric, the interfacial contours of only one-half of the interface are shown as insets in Fig. 2. The pattern that develops is clearly dendritic. This pattern evolved solely under the influence of the GTH boundary condition, without any significant noise present. The lack of noise and high accuracy are ensured by the fact that this method is spectrally accurate, and, moreover, that the heat flux maintained is well below that for which noise from the discretization, and rounding errors, could be significantly amplified during the computation time. In addition, equivalent patterns with coherent side branches evolved for a variety of starting shapes, including just starting with the equilibrium Wulff shape. Neither the spatio-temporal coherence of the branches was imposed, nor was the starting two-fold symmetry enforced in these calculations.

The details of how a side branch is initiated and grows can be seen in Figs. 2 and 3. In Fig. 2, the velocity $\bar{V}$ of the tip of the x-primary arm in the scaled frame of reference is plotted as a function of $\bar{R}$; the tip velocity V in the unscaled (true) frame of reference is shown as an inset. From Fig. 3, it is seen that the local maxima in $\bar{V}$ correlate consistently with the development of non-monotonic temperature distributions near the tip, and the initiation of side branches. Interestingly, these oscillations are not easily observable in the true tip velocity, as they are submerged within the overall growth dynamics. Thus, we contend that an accurate numerical method, capable of separating the dynamics of growth from those of shape change, is required to expose and capture the underlying phenomena of side branch formation.

In Fig. 3[a]–[f], sequences of interface morphologies and associated interface temperature distributions are shown. What is observed is that despite the lack of any noise or other imposed interfacial disturbances, the interface becomes negatively curved in perfect synchrony with the interfacial temperature becoming non-monotone near the tip. Non-monotonicity of the temperature near the tip is observed to occur periodically, further suggesting that the operation of a "limit cycle," rather than selective amplification of noise, provides the dynamical mechanism for dendritic side branching.

The operation of the dendritic limit cycle involves progressive shape changes near the tip that eventually induce a non-monotonic temperature distribution. This leads to the development of a protuberance, changes in the sign of the interface curvature, and, eventually, the formation of a side branch as shown in Fig. 3[a]–[f]. The cycle then repeats.

The initial needle-like elliptical shape, Fig. 3[a], has a monotonic temperature distribution as the tip is approached ($\alpha \to 0^{\pm}$). In Fig. 3[b] the advancing tip becomes less curved, and the interfacial temperature distribution changes. In Fig. 3[c], a pair of local temperature maxima develop near

$\alpha \approx \pm 0.15$. Although it is not apparent yet from the interface shape at the resolution shown, the interface curvature changes sign near the temperature maxima that give rise to a small protuberance that will later grow into a side branch. In Fig. 3[c] a small protuberance is now seen, and new local maxima in the temperature have developed near $\alpha \approx \pm 0.075$. New protuberances form each time the temperature distribution becomes non-monotonic. Both protuberances at $\alpha \approx \pm 0.15$ and $\alpha \approx \pm 0.075$ can be clearly seen in Figs. 3[d] and 3[f] as they grow and negative curvature develops. As may be inferred from Fig. 3[f], new local maxima in the temperature are going to occur at $\alpha \approx \pm 0.04$ and new protuberances will be produced. This cycle is repeated indefinitely as suggested by the overall solidification pattern, Fig. 2.

Discussion and Summary

A careful analysis of the Gibbs-Thomson-Herring (GTH) boundary condition shows that "shape anisotropy", i.e., an elongated shape in one spatial direction, combined with interfacial energy anisotropy can lead to non-monotone equilibrium temperature distributions. The specific case of the parabola—a one-parameter conic section—was analyzed in this paper. It was shown that non-monotone behavior occurs at the tip of a parabola if the anisotropy parameter in the GTH boundary condition, $\eta \geq 1/95 \approx 0.0105$. Other needle-shapes, such as an ellipse—a two-parameter conic section—evolve similarly, despite their mathematical differences from the parabola, with the non-monotone behavior depending both on the shape (C/A ratio) and the energy anisotropy, η. A sequence of non-monotonicities in temperature occurs close to the tip, and as our sharp-interface simulations show, the temperature field interacts dynamically with the evolving shape. It appears that each time local temperature maxima occur, curvature oscillations develop slightly aft of the tip. These curvature oscillations stimulate the formation of a pair of protuberances, which in most cases continue to grow and form opposing, coherent side branches. Experimental observations, such as accomplished in the IDGE, seldom reveal coherent side branching, but this fact might simply be caused by the fact that the thermal fields during dendritic growth are never perfectly symmetrical about the growth axis. Also, what seems especially significant about these simulations of dendritic pattern formation is that perturbations to the crystal-melt interface, and so-called selective amplification of noise, play no rôle in the process. The GTH boundary condition itself seems to provide a deterministic boundary condition that, when combined with sufficient shape and energy anisotropies, is fully capable of inducing a dynamic limit cycle near the tip. The origin of dendritic side branching might be quite different from current conventional concepts.

If the mechanism of dendritic growth in three-dimensions behaves similarly—and we have initial theoretical evidence that it does [21]—then the subject of dendritic growth dynamics will require a thorough re-investigation of its basic cause. Currently accepted theoretical paradigms that purport to explain dendrite behavior use morphological stability theory, based on linear perturbative methods [9], or appeal to solvability methods [10]. The pattern formation mechanism uncovered here relies on nothing more than the GTH boundary condition combined with an interface shape that has sufficient anisotropy, i.e., sufficiently steep curvature gradients. Other interesting morphological phenomena concerning the directional solidification of alloys, such as the cell-to-dendrite transition, and the relationship of side branch spacings to the solidification parameters might also require re-interpretation based on the non-monotonic behavior of the GTH boundary condition disclosed herein.

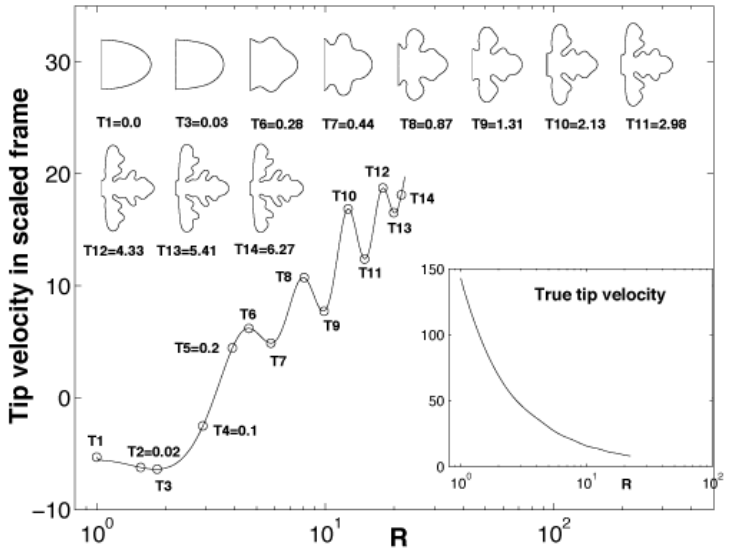

Figure 2: Boundary integral simulation of the evolution of an elliptical interface with a shape anisotropy $C/A = 2$, a surface energy anisotropy of $\eta = 0.005$ and a constant far-field heat flux. The crystal morphologies (one-half) are shown as insets. The scaled velocity, $\bar{V}$, at the tip and the unscaled (true) tip velocity, V, are also shown. The evolution periodically generates side-branches when the temperature distribution near the tip becomes non-monotonic. These are reflected in the oscillations of $\bar{V}$. The tip grows faster than the surrounding interface, and subsequent negative curvatures are initiated at various locations along the interface where the temperature periodically becomes non-monotonic, suggestive of a dynamic limit cycle.

References

[1] G.P. Ivantsov, *Dokl. Akad. Nauk. USSR*, **558**,(1947) 567.

[2] M.E. Glicksman, R.J. Schaefer, and J.D. Ayers, *Metall. Trans. A*, **7**,(1976) 1747.

[3] G.E Nash and M.E. Glicksman, *Acta Metall.* **22** (1974) 1283.

[4] G.E. Nash and M.E. Glicksman, *Acta Metall.* **22** (1974) 1291.

[5] W. Oldfield, *Mater. Sci. Eng.* **11** (1973) 211.

[6] R.D. Doherty, B. Cantor, S. Fairs, *Metall. Trans.* **A 9** (1978) 621.

[7] M.E. Glicksman, S.P. Marsh, "The Dendrite" *Handbook of Crystal Growth*. Ed. D. Hurle, Elsevier Science Publishers, Amsterdam, (1993) 1075-1122.

[8] M.E. Glicksman and A.O. Lupulescu,"Dendritic Crystal Growth in Pure Material", *J. Crystal Growth*, 264, 4, (2004) 541-549.

[9] J.S. Langer and H. Müller-Krumbhaar, *J. Crystal Growth*, **42**, (1977) 11.

[10] D. Kessler and H. Levine, *Phys. Rev. A*, **36**, (1987) 4123-4126.

[11] D. Kessler and H. Levine, *Phys. Rev. B* **33** (1986) 7867.

[12] D. Kessler and H. Levine, *Phys. Rev. Lett.* **57** (1986) 3069.

[13] D. Kessler and H. Levine, *Acta Metall.* **36** (1987) 2693.

[14] A. Barbieri and J.S. Langer, *Phys. Rev. A*, **39**, (1989) 5314.

[15] W.W. Mullins and R.F. Sekerka,*J. Appl. Phys.* **34** (1963) 323.

[16] M.E. Glicksman, M.B. Koss, and E.A. Winsa, *Phys. Rev. Lettrs.*, **73**, No. 4 (1994) 573.

[17] J.C. LaCombe, M.B. Koss, V.E. Fradkov, M.E. Glicksman, *Physical Review, E*, **52**, No. 3, (1995) 2778.

[18] T.Y. Hou, J.S. Lowengrub and M.J. Shelley, *J. Comput. Phys.*, **114**, (1994) 312.

[19] S. Li, J.S. Lowengrub, P.H. Leo, and V. Cristini, *J. Crystal Growth*, **277**, (2005) 578.

[20] S. Li, J.S. Lowengrub, and P.H. Leo, *Physica D*, **208**, (2005) 209.

[21] G.F. McFadden and S.R. Coriell, Private communication, 2005.

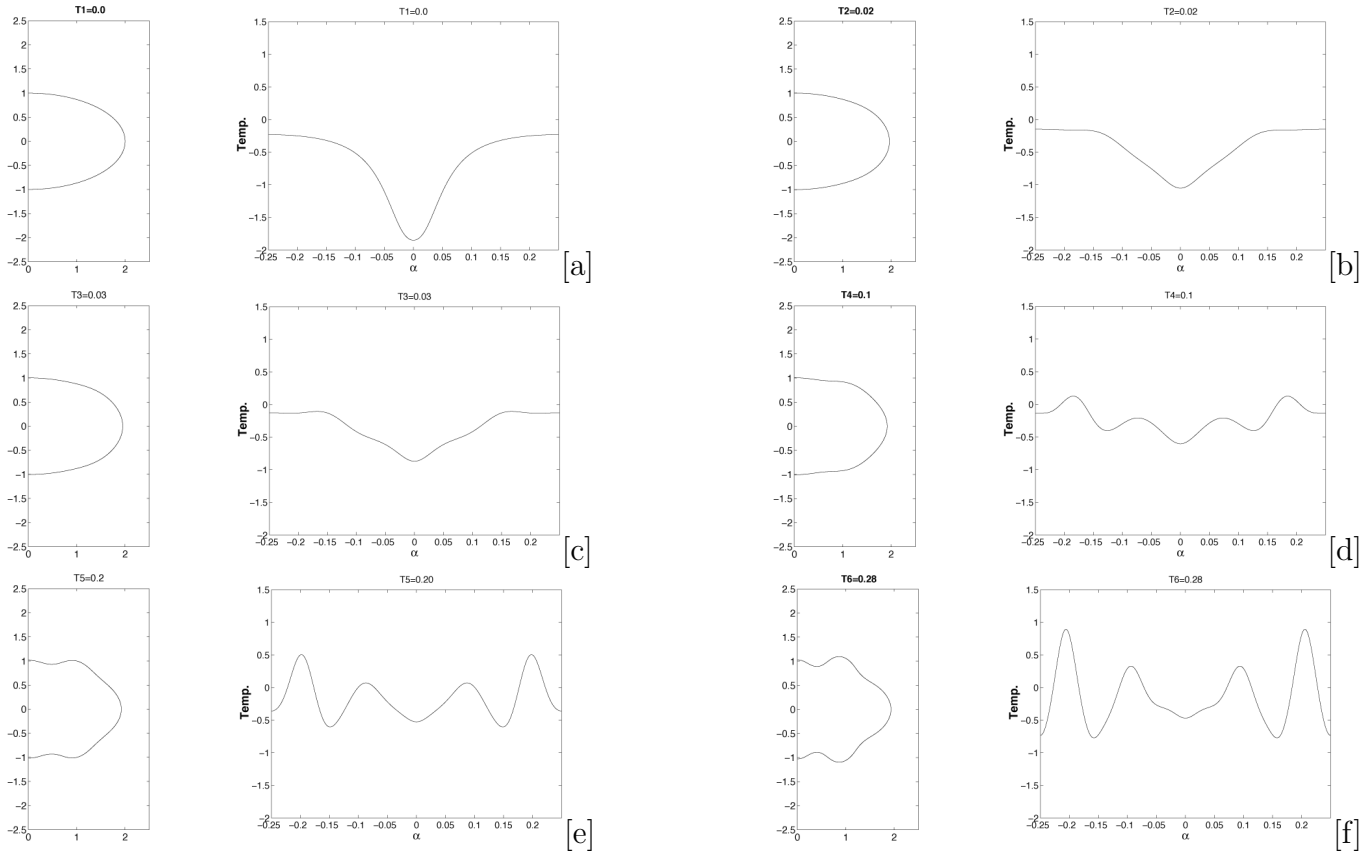

Figure 3: *Details of the development of side branches during evolution of the initially elliptical interface shown in Fig. 2, suggestive of the operation of a "limit cycle".* **[a]** $T = 0$**:** *Starting ellipse, with a monotone-down interface temperature as the tip,* $\alpha \to 0^-$ *is approached.* **[b]** $T2 = 0.02$**:** *Tip becomes slightly less curved than in [a] and the temperature shift lessens.* **[c]** $T3 = 0.03$**:** maxima in the temperature develop near $\alpha \approx \pm 0.15$. **[d]** $T4 = 0.1$**:** *Small protuberances develop in the morphology (near* $\alpha \approx \pm 0.15$*), and additional maxima in the temperature appear near* $\alpha = \pm 0.075$. **[e]** $T5 = 0.2$**:** and **[f]** $T6 = 0.2$**:** *Negative curvatures form ahead of the growing protuberances, and additional new temperature maxima develop yet closer to the tip at* $\alpha \approx \pm 0.04$*—about* 10° *off the tip orientation—in anticipation of the formation of the next protuberance.*

Acknowledgement

JSL and SL acknowledge support from the National Science Foundation (DMS) and the University of Minnesota, Sponsored Projects Office. MEG is grateful for his support provided through the John Tod Horton Distinguished Professorship of Materials Science and Engineering. Thanks are also extended to the National Aeronautics and Astronautics Administration, NASA, Washington, DC, for their financial and operational support of the Isothermal Dendritic Growth Experiment (IDGE).